DOI: https://doi.org/10.15446/ing.investig.116327

Research Article/ Civil and Sanitary Engineering

Empirical Models for the Shear Capacity and Stiffness of X-Shaped Screw Connections in Timber-Concrete Composite Structures

Modelos empíricos de resistencia al cortante y rigidez para conexiones de tornillos en X en estructuras compuestas de madera-concreto

Mohd Amirul Mohd Snin[1], Anis Hanim Ghazali[2], and Deng Haolin[3]

ABSTRACT

In the literature, experimental data on X-shaped screw connections have been analyzed in order to develop an empirical model for their shear force capacity and stiffness, which are important parameters in designing timber-concrete composite structures. Although considerable research has been conducted worldwide to understand the composite action of timber and concrete, there is no generic model for determining the shear force capacity and stiffness of screw connections; most of the existing models are based on theoretical derivations. In this paper, empirical models are derived to determine the shear capacity of screw connections installed in X-shaped arrangements, considering the embedment and withdrawal strength of the screws within the timber and concrete. Moreover, a stiffness model based on global flexibility, as influenced by the material properties of timber, concrete, and screws, is elaborated. The model is validated using existing push-pull data and variations in material properties. A comparison with a well-known model demonstrates the suitability of our proposal. This model can be used to predict the shear force capacity and stiffness of X-shaped screw connections in timber-concrete composite structures.

Keywords: timber-concrete composite structures, timber structures, timber connections

RESUMEN

En la literatura se han analizado datos experimentales sobre las uniones con tornillos en X, a fin de desarrollar un modelo empírico de su resistencia al cortante y rigidez, parámetros importantes en el diseño de estructuras compuestas de madera-concreto. Aunque se ha llevado a cabo una cantidad considerable de investigaciones a nivel mundial para comprender la acción compuesta de la madera y el concreto, no existe un modelo genérico para determinar la resistencia al cortante y la rigidez de las uniones con tornillos; la mayoría de los modelos existentes se basan en derivaciones teóricas. En este trabajo se derivan modelos empíricos para determinar la resistencia al cortante de las uniones con tornillos en X, considerando la resistencia al empotramiento y al arranque de los tornillos en la madera y el concreto. Además, se elabora un modelo de rigidez basado en la flexibilidad global, influenciada por las propiedades de los materiales de la madera, el concreto y los tornillos. El modelo se valida utilizando datos experimentales de ensayos *push-pull* y variaciones en las propiedades de los materiales. Una comparación con un modelo reconocido demuestra la idoneidad de nuestra propuesta. Este modelo puede emplearse para predecir la resistencia al cortante y la rigidez de las uniones con tornillos en X en estructuras compuestas de madera-concreto.

Palabras clave: estructuras compuestas de madera y concreto, estructuras de madera, conexiones de madera

Received: August 23rd, 2024
Accepted: July 21st, 2025

Introduction

The timber-concrete composite (TCC) system, introduced in Germany around 100 years ago, has gained significant traction in flooring applications over the past 20-30 years [1]. TCC structures, which are one-way spanning elements subject to uniaxial bending, combine timber beams with concrete slabs to leverage timber's tensile strength and concrete's compressive strength [2], [3]. This composite system generally outperforms timber-only systems in flooring applications [4], [5]. Shear connections are crucial for providing ductility, with their design parameters (strength, stiffness, deflection, and configuration) being critical to the overall performance of TCC systems [1], [6], [7], [8]. Research indicates that the material properties of timber, concrete, and fasteners significantly affect shear capacity and stiffness [9], [10]. Inclined fasteners enhance stiffness and strength more effectively than vertical ones,

[1]PhD in Civil Egineering , University of Bristol, United Kingdom. Affiliation: senior lecturer, Universiti Sains Malaysia, Malaysia. Email: ceamirul@usm.my

[2]Bachelor in Civil Engineering, Universiti Sains Malaysia, Malaysia. Affiliation: master student, Universiti Sains Malaysia, Malaysia. Email: anishanim1@student.usm.my

[3]Bachelor in Civil Engineering, Yangtze Normal University, China. Affiliation: master student, Universiti Sains Malaysia, Malaysia. Email: holyd1020x@163.com

with screws being favored for their high load-bearing capacity and ease of installation [11], [12].

In particular, the use of X-shaped screw arrangements —meaning that two screws are installed at opposing angles to form a cross or X through the interface— has been shown to significantly enhance the mechanical performance of composite joints. This configuration improves the connection's ability to resist shear forces and increases the overall joint stiffness by enabling a more efficient transfer of loads between the connected materials. The experimental and theoretical research conducted by [13] in timber-to-timber composite systems confirmed that X-shaped screw arrangements outperform their parallel or perpendicular counterparts in terms of both load-bearing capacity and stiffness. Specifically, inclined screws positioned in this X-shaped arrangement create a self-reinforcing action that restrains slip and distributes forces more uniformly along the interface.

The benefits observed in timber-to-timber composites imply that similar advantages could be attained in TCC systems, where efficient shear transfer and stiffness are also critical. Although TCC systems involve different material interactions (between timber and concrete), the underlying principle of improved mechanical interlock and force transfer remains relevant. Therefore, adopting X-shaped screw arrangements in TCC applications could potentially enhance the overall structural performance, especially regarding shear capacity, stiffness, and ductility at the timber-concrete interface [14], [15]. This promising potential motivates further investigation into the application of X-shaped screw configurations in TCC structures [13], [16]. In [17], the authors delved into the shear performance of inclined X-shaped screw arrangements in nail-laminated timber-to-concrete composite floors. They found that the shear capacity and stiffness increased significantly compared to the parallel-in-compression arrangement. Moreover, [18] compared the shear performance of glued steel plate connections in TCC and X-shaped arrangements, concluding that the latter provide higher ductility and stiffness.

Eurocode 5 [19] provides guidelines for vertical fasteners but lacks comprehensive analytical equations for predicting the shear capacity and stiffness of TCC connections with inclined screws. This research analyzes the effects of screw inclination on shear capacity and stiffness using a dataset from published studies, in addition to developing a predictive model for inclined screws in X-shaped arrangements.

Methodology

Empirical method used

This paper outlines the use of empirical methods to predict the shear capacity and stiffness of TCC structures. This analysis leverages a database of shear test results from previous studies on TCC specimens, focusing on crucial parameters for designing timber-concrete connections, including the size, formation, type, and mechanical properties of the fasteners. Moreover, multiple linear regression (MLR) is employed to predict shear capacity and stiffness. The key factors considered include the distance between the hinge and the timber-concrete interface, which affects screw embedment strength, and properties such as concrete/timber strength (σ_s/σ_B), fastener length (L_c), diameter (D), screw strength ($\sigma_{y(s)}$), and the inclination angle of the screw (θ). Notably, larger fastener diameters and longer fasteners have been shown to enhance shear capacity [20], [21], [22], and the concrete slab type significantly impacts this parameter [23]. In summary, this study collects and analyzes shear test data using MLR to develop predictive models for the shear capacity and stiffness of screw connections.

Fundamentals of the longitudinal shear capacity of fasteners

The shear capacity (P_{max}) of screw connections is influenced by the axial loading (P_a) on the screw (also known as the *withdrawal strength*), and the force applied due to embedment strength P_b, as shown in Eq. (1). Eurocode 5 [19] provides methods to estimate both P_a and P_b for screws in timber. However, similar guidelines for timber-concrete connections are lacking.

$$P_{max} = P_a + P_b \tag{1}$$

Withdrawal strength of screws in TCC structure specimens

Each screw is partially embedded into both the concrete and the timber. Under an applied force, the screws tend to withdraw either from the concrete or the timber. The withdrawal strengths of timber ($P_{a(t)}$) and concrete ($P_{a(c)}$) are considered in calculating the shear capacity of the connection, as per Eurocode 5 [19]. [24] highlighted the significant contribution of axial loading to the shear capacity. Their research found that the axial load on specimens with a 45° inclination angle was higher compared to those at 60° and 75°. They also noted that this parameter is influenced by the screw's inclination angle. In their study, the inclination angle was measured between the timber-concrete interface and the screw's position. The axial load increased as the angle decreased from 90° to 45°.

The withdrawal strengths of timber and concrete are calculated based on the shear strength and tensile strength of the respective materials, as shown in Eqs. (2) and (3) [25], [26]. Notably, the experimental results of [24] were obtained from double-shear test specimens. To calculate the shear capacity, the lowest withdrawal strength value from Eqs. (2) and (3) is used. In both equations, L_t represents the length of the screw embedded in timber, and L_c denotes the length of the screw embedded in concrete.

$$P_{a(t)} = 0.2\ \pi D L_t {\sigma_B}^{0.8} \cos\theta \tag{2}$$

$$P_{a(c)} = 0.3 \pi D L_c {\sigma_S}^{0.67} \cos\theta \tag{3}$$

Embedment strength of the screw in timber-concrete composite structures

In Eurocode 5 [19], embedment strength is determined using Clause 8.3.1.1, which applies solely to timber. This equation calculates the embedment strength of screw connections based on the full length of the screw embedded in the timber. The embedment strength in concrete is also addressed by [19], albeit assuming that the embedment strength of the screw is three times the concrete's strength. It is also mentioned that the length of the screw should be at least three times the screw diameter. However, our formulation builds upon the concepts of [27]. Fig. 1 illustrates how the hinge mechanism in concrete reacts to bending forces. According to [27], the shear capacity depends on either the timber bearing capacity ($f_{h,t}$) along the effective length (l_t) or the concrete bearing stress ($f_{h,c}$) along the effective length (l_c). The maximum bending moments occur at points A and B (Figure 1c), leading to an equilibrium state (Figure 1d). [27] proposed Eq. (8) to calculate P_b for a 90° screw. Furthermore, [24] observed that a higher screw inclination angle (from 45° to 90°) reduces the distance between the hinge and the timber-concrete interface. They provided parameters for this distance for screws in concrete — Eqs. (4) and (5)— and in timber —Eqs. (6) and (7). For screws in concrete, the force caused by the embedment strength is given by

Eq. (8), where the effective area is $D \times (L_c - l_c)$. Eq. (9) simplifies this, and Eq. (10) accounts for various screw angles. The screw angle affects $f_{h,c}$, which must be adjusted based on the angle in order to determine its value along the X-axis.

For tension:

$$l_c = 0.0031\theta L_c - 0.11L_c \quad (4)$$

For compression:

$$l_c = 0.50L_c - 0.0040\theta L_c \quad (5)$$

For tension:

$$l_t = -0.0117\theta L_t + 1.13L_t \quad (6)$$

For compression:

$$l_t = -0.0041\theta L_t + 0.43L_t \quad (7)$$

$$P_b = f_{h,c}D(L_c - l_c) \quad (8)$$

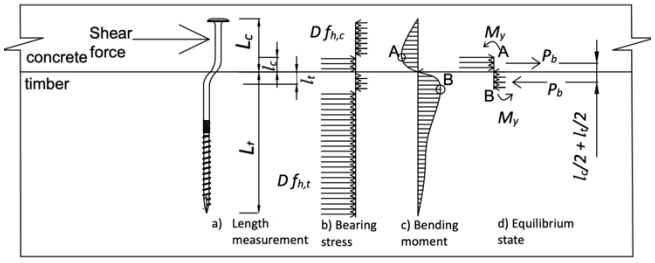

Figure 1. Hinge mechanism in concrete
Source: Authors

$$f_{h,c} = \frac{P_b}{D(L_c - l_c)} \quad (9)$$

$$f_{h,c} = \frac{P_b}{D(L_c - l_c)} \sin\theta \quad (10)$$

Developing an empirical shear capacity and stiffness model

This subsection details the development of empirical models for shear capacity and stiffness using MLR. Initially, the limitations of the model by [27] were noted, specifically associated with its failure to consider screw angles. According to [24], the effective length (l_c) varies with the screw angle: it decreases for compression screws and increases for tension screws as the angle increases from 45° to 90°. This analysis involves parameters such as P_{max}, P_a, P_b, D , L_c , L_t ,l_c , $\sigma_{y(s)}$, σ_s, and σ_B. In this work, the unknown parameter $f_{h,c}$ was analyzed through MLR, and the empirical model for $f_{h,c}$ was then used in the equation for P_{max}. As for stiffness, the existing model by [1] exhibits some limitations for a 90° screw angle. This study proposes a new stiffness model based on the equation of K_s. The global flexibility coefficient (J), an unknown value, was analyzed using MLR with the known parameters K_s, E_s, and I_s. The empirical model for J was then substituted back into the equation for K_s, resulting in a new stiffness model.

Database of connection specimens

The process of deriving the predictive model for shear force capacity and stiffness began with the collection of data from previous studies. Table I presents the compiled data on shear force connection tests from various sources, and Table II shows the overall range of properties for all specimens. All specimens analyzed were tested in an X-shaped arrangement. The sources were selected based on connection tests using TCC, corresponding to the 2014-2023 period. A total of 60 specimens was included, comprising both single- and double-shear test specimens (see Appendix I in the supplementary material for full details).

Table I. Database of connection shear tests from 2014 to 2023

Reference	Test	No. of samples	Sample properties					
			D (mm)	L_s (mm)	σ_B (MPa)	σ_S (MPa)	σ_y(s) (MPa)	θ (°)
[1]	Single shear	12	7.5	65-97	48	28	510	30-60
[23]	Double shear	2	6	210	70	32.7	1100	45
[20]	Double shear	12	8-16	100-120	44.9	49.7	1200	90
[28]	Double shear	12	8-12	160	24	32.7	160	45
[29]	Double shear	10	10-14	180	43.4	40-60	462	30-90
[30]	Double shear	4	11	150-200	39	32	504	30-45
[24]	Double shear	8	6	210	24-70	16.36-26.5	820	30-90

Source: Authors

Table II. Ranges in the database

Parameters	Range
Screw diameter – D	6-16 mm
Screw length – L_s	65-210 mm
Beam strength (timber) – σ_B	24-70 MPa
Slab strength (concrete) – σ_S	16.36-60 MPa
Screw angle – θ°	30-90°
Number of specimens	60

Source: Authors

Results and discussion

Influence of material properties on the embedment strength of screws in concrete

This subsection addresses the influence of material properties on the embedment strength of screws in concrete. Fig. 2 plots the concrete embedment strength ($f_{h,c}$) against the distance between the hinge and the timber-concrete interface (l_c). This graph shows the measured $f_{h,c}$ values of 60 specimens, with power laws fitted to the data. The coefficient of determination (R^2) for the plot is 0.6616, indicating a quite significant relationship between l_c and $f_{h,c}$. The analysis reveals that the embedment strength of screws in concrete decreases as l_c increases. The shear capacity consists of two components: the force from the withdrawal strength and the force from the embedment strength, as expressed in Eq. (1). The withdrawal strength is higher for smaller screw angles, while the embedment strength increases with larger screw angles. In conclusion, the primary factor affecting the embedment strength of screws within concrete is l_c.

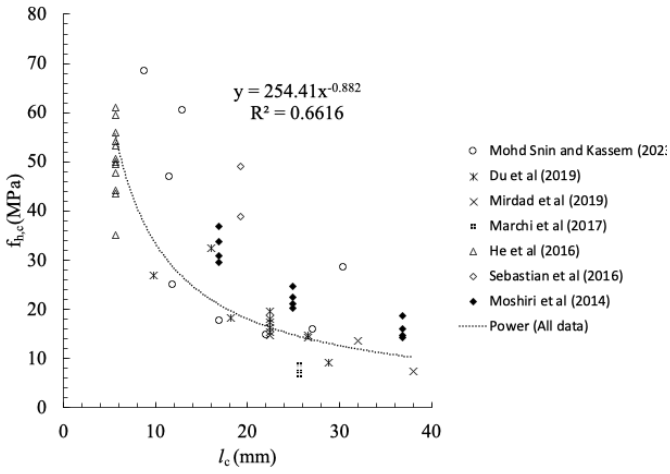

Figure 2. $f_{h,c}$ plotted *vs.* timber beam strength
Source: Authors

Mathematical model for the embedment strength of screws in concrete

The most influential factor affecting the embedment strength of screws in concrete is the distance between the hinge and the timber-concrete interface. This factor was used as the primary parameter in developing the mathematical model for $f_{h,c}$. An MLR analysis was performed to develop a combined equation that incorporated an additional parameter (σ_B) to predict $f_{h,c}$. This is presented in Eq. (11) in logarithmic form. This equation was simplified to form Eq. (12), which was used to plot the linear graph. Additionally, Eq. (13) presents a simplified expression for calculating the value of $f_{h,c}$. The terms m and n are the exponents for σ_B and l_c, respectively.

$$ln\left(f_{h,c}\right) = mln(l_c) + nln(\sigma_B) + C \quad (11)$$

$$\frac{ln(f_{h,c})}{ln\left(\sigma_B{}^n\right)} = ln(l_c{}^m) + C \quad (12)$$

$$f_{h,c} = C l_c{}^m \sigma_B{}^n \quad (13)$$

Optimizing the mathematical model for the embedment strength of screws in concrete

To optimize Eq. (13), it is necessary to determine the best values for *m and n*. An analysis was conducted to obtain the exponents for each variable in the equation. This was done by including two variables: l_c and σ_B. Table III presents the results. Here, the R^2 value improved to 0.90, the standard error was further reduced to 0.227, and the optimal exponents *m* and *n* were found to be -0.68 and 1.2 for l_c and σ_B. Based on all analyses conducted in relation to $f_{h,c}$, it was confirmed that l_c and σ_B have a significant effect on Eq. (14), which is presented below. Plots of the measured *vs.* predicted $f_{h,c}$ values were generated to assess this effect. Fig. 3 presents the plot for the model incorporating σ_B and l_c. This plot shows that almost 90% of the TCC specimen data fall within ± 33% of the line of equality. From these plots, it can be concluded that Eq. (14) provides better predictions.

$$f_{h,c} = 1.73 l_c{}^{-0.68} \sigma_B{}^{1.2} \quad (14)$$

Table III. MLR results of $f_{h,c}$ for compression fasteners – ANOVA: MS Excel for Eq. (14)

Regression statistics	
Multiple R	0.94938067
R squared	0.90132366
Adjusted R squared	0.89786133
Standard error	0.22732942
Observations	60

Source: Authors

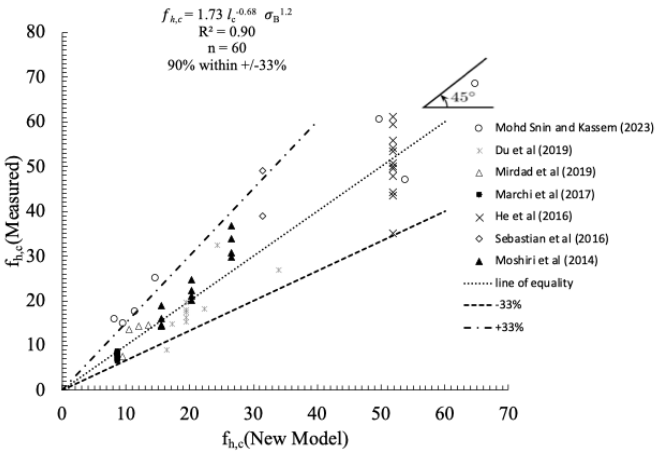

Figure 3. Plot of measured *vs.* predicted $f_{h,c}$ for compression screws
Source: Authors

Finalizing the new shear capacity model

In the above-presented MLR analysis, the equations for the $f_{h,c}$ of compression screws were developed. Based on Eq. (1), the total shear capacity of the connection is the sum of P_b plus P_a. P_b can be determined by substituting the empirical equation for $f_{h,c}$ into Eq. 10. The complete equation for P_b is presented in Eq. (15). This expression is then substituted into Eq. (1) to derive the full shear capacity formula, as shown in Eqs. (16) and (17).

$$P_b = \frac{1.73 l_c{}^{-0.68} \sigma_B{}^{1.2} D(L_c - l_c)}{\sin\theta} \quad (15)$$

$$P_{\max} = 0.2\,\pi D L_t \sigma_B{}^{0.8} \cos\theta + \frac{1.73 l_c{}^{-0.68} \sigma_B{}^{1.2} D(L_c - l_c)}{\sin\theta} \quad \textbf{If } P_{a(t)} < P_{a(c)} \quad (16)$$

$$P_{\max} = 0.3\pi D L_c \sigma_S{}^{0.67} \cos\theta + \frac{1.73 l_c{}^{-0.68} \sigma_B{}^{1.2} D(L_c - l_c)}{\sin\theta} \quad \textbf{If } P_{a(c)} < P_{a(t)} \quad (17)$$

Developing the mathematical model for stiffness

The stiffness model presented in this study was developed based on the theory of [27]. The equation provided in the cited reference was modified by neglecting the plank wood thickness of the TCC specimens, resulting in Eq. (18). The flexibility coefficients in this equation were simplified into a single variable parameter, *J*, which denotes the global flexibility coefficient. This is shown in Eqs. (19) and (20).

$$K_s = \frac{12(\alpha_c \alpha_t)^3 E_s I_s}{3(\alpha_c^2 + \alpha_t^2)(\alpha_c + \alpha_t)} \quad (18)$$

$$K_s = 4 J E_s I_s \quad (19)$$

$$J = \frac{(\alpha_c \alpha_t)^3}{(\alpha_c^2 + \alpha_t^2)(\alpha_c + \alpha_t)} = \frac{K_s}{4 E_s I_s} \quad (20)$$

where:

- α_c = distance between the center of the concrete member and the neutral axis
- α_t = distance between the center of the timber member and the neutral axis
- E_s = Young's modulus of the screw
- I_s = moment of inertia of the screw

Influence of material properties on the global flexibility coefficient of screws in the concrete

The mechanical properties of screw connections in TCC structures significantly affect their stiffness. This section discusses the factors influencing the global flexibility coefficient of said connections. A plot of this coefficient *vs.* screw diameter is presented in Fig. 4. The plot shows an R^2 value of 0.7016, indicating that diameter has a substantial effect on *J*. Additionally, the plot demonstrates that the global flexibility coefficient decreases as the screw diameter increases.

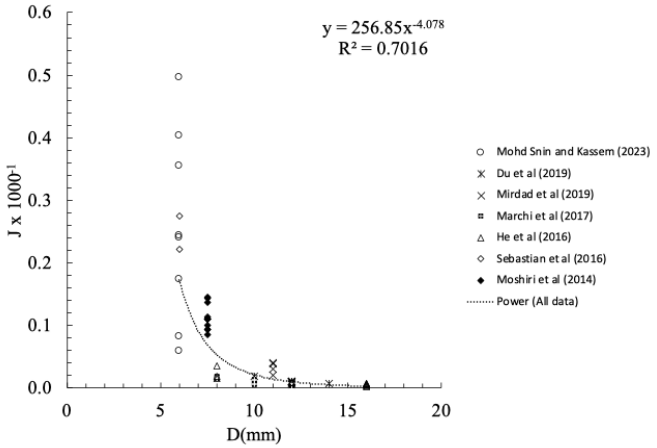

Figure 4. Global flexibility coefficient *vs.* diameter
Source: Authors

Mathematical model for the global flexibility coefficient

The factors influencing the global flexibility coefficient were discussed in the previous subsection. This coefficient was used as the main parameter in the MLR analysis to derive the empirical model. The mathematical model for this primary parameter is presented in Eq. (21) in logarithmic form. This equation was simplified into Eq. (22), where the terms *m, n, k*, and *p* represent the exponents of the screw diameter, beam compressive strength, slab compressive strength, and angle, respectively.

$$ln\,(J) = mln(D) + nln(\sigma_B) + kln(\sigma_S) + pln(\theta) + C \quad (21)$$

$$J = CD^m {\sigma_B}^n {\sigma_S}^k \theta^p \quad (22)$$

Optimizing the mathematical model for J

This subsection focuses on optimizing the exponent values for each of the previously discussed parameters. The MLR analysis was conducted using MS Excel, as with the mathematical model for the embedment strength of screws in concrete, and it included four parameters: *D*, σ_B, σ_S, and θ —see Eq. (22). Based on this analysis, the exponents *m, n, o*, and *p* were determined to be -2.5, 1.62, -1.64, and -0.52, respectively (Table IV). The coefficient *C* was found to be 0.05. Additionally, the R^2 value improved to 0.895, and the standard error decreased to 0.48. The complete formula for *J* is presented in Eq. (23). Plots of the measured *vs.* the predicted *J* were generated according to (23) in order to assess how material properties influence this parameter. When the diameter, beam strength, slab strength, and angle were all included in this equation, the percentage of data samples within the ± 33% margin of the line of equality improved to 90% (Fig. 5).

$$J = 0.05D^{-2.5}{\sigma_B}^{1.62}{\sigma_S}^{-1.64}\theta^{-0.52} \quad (23)$$

Table IV. MLR results for *J* – ANOVA: MS Excel for Eq. (23)

Regression statistics	
Multiple R	0.94594156
R squared	0.89480544
Adjusted R squared	0.88715493
Standard error	0.48033232
Observations	60

Source: Authors

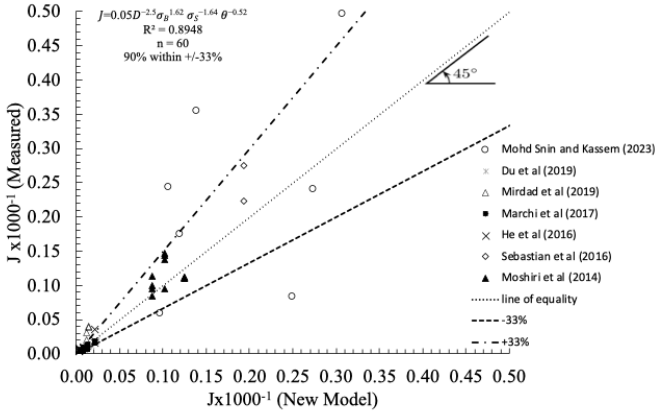

Figure 5. Plot of measured *vs.* predicted *J* for compression screws
Source: Authors

The final stiffness formula was derived by substituting (23) into (19), resulting in Eq. (24).

$$K_s = \frac{0.2{\sigma_B}^{1.62}E_sI_s}{D^{2.5}{\sigma_S}^{1.64}\theta^{0.52}} \quad (24)$$

Comparing the new model to existing published works

The newly developed predictive models for shear capacity and stiffness were validated by comparing them against existing published models. The database used for this validation is presented in Table I. The models proposed by [31] and [1] are the only ones that consider the shear capacity and stiffness of X-shaped screw connections in TCC structures. They are presented in Eqs. (25) and (26), respectively. These models were used as benchmarks to evaluate our proposal.

$$P_{max} = f_{h,t,\theta}DL_tcos\theta + \frac{\pi DL_tf_{ax,t,\theta}}{sin\theta} \quad (25)$$

$$K_s = \frac{E_SA_S}{\sqrt{\frac{(1+\beta tan^3(90-\theta)E_SA_Scos(90-\theta)}{k_p\beta tan(90-\theta)}}}tanh\frac{L_t}{\sqrt{\frac{(1+\beta tan^3(90-\theta)E_SA_Scos(90-\theta)}{k_p\beta tan(90-\theta)}}} \quad (26)$$

where:

- $f_{ax,t,\theta}$ = axial withdrawal load in timber
- $f_{h,t,\theta}$ = embedment strength of timber

- E_s = Young's modulus of the screw
- β = ratio between the embedment strengths of concrete and timber
- k_p = foundation modulus of timber in parallel

Comparison of the shear capacity models

This subsection compares the results obtained from our proposal and those from the model by [31]. Plots of measured *vs.* P_{max} were created for both models. As shown in Fig. 6, the new empirical model exhibits an R^2 value of 0.82, with 97% of the data samples falling within ±33%. This indicates that our proposal offers good shear capacity predictions. On the other hand, Fig. 7 presents the same plot for the model by [31]. Here, the values correspond to the closest approximation to the measured P_{max}. The plot reveals an R^2 value of 0.544, significantly lower than that of the new empirical model. Additionally, only 73% of the data samples fall within ±33% of the line of equality.

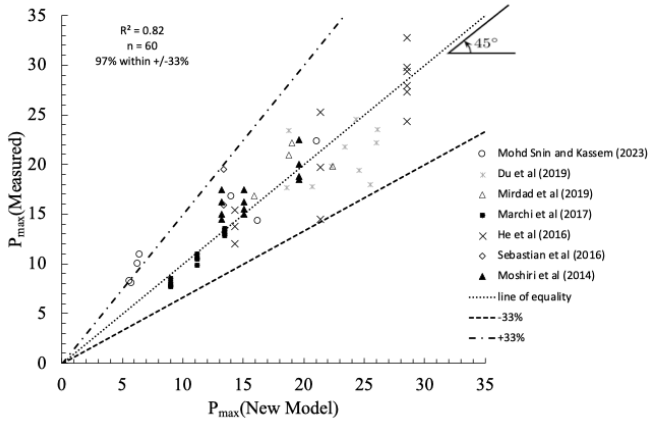

Figure 6. Measured *vs.* predicted P_{max} for the new empirical model
Source: Authors

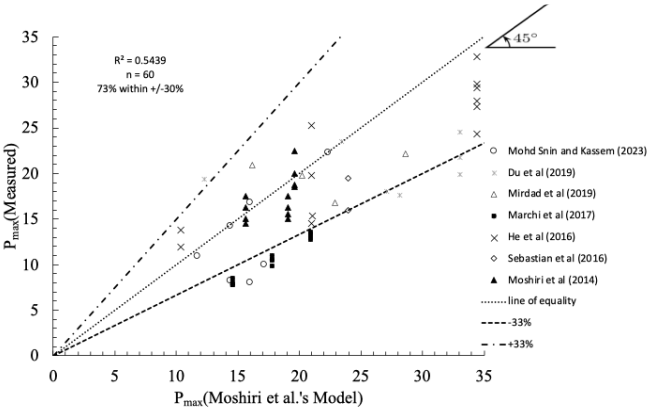

Figure 7. Measured *vs.* predicted P_{max} for the model by [31]
Source: Authors

We generated a plot of the ratio between the measured and the model's P_{max} *vs.* the angle to compare the two models (Fig. 8). It is evident that the new empirical model provides a closer prediction than [31]. The mean and standard error of our proposal are 0.99 and 0.17, respectively. In contrast, the model by [31] reports a mean and a standard error of 1.30 and 0.35, which are higher than those of the new model. Furthermore, the plot shows that the ratio for all data samples using the new empirical model falls within the range of 0.5 to 1.5. Meanwhile, the ratio for the other model encompasses a wider range, from 0.5 to 2.1. This demonstrates that our proposal outperforms the model in [31] when it comes to predicting shear capacity.

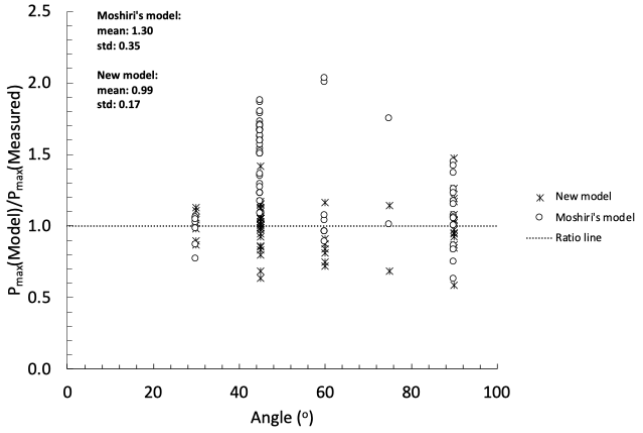

Figure 8. Modeled/measured P_{max} *vs.* screw angle
Source: Authors

Stiffness model comparison

This subsection compares our stiffness model against that of [1]. Plots of measured *vs.* predicted K_s were generated for both models. Fig. 9 presents the plot for the new empirical model, showing an R^2 value of 0.3425. Approximately 67% of the data samples fall within ± 33% of the line of equality. As for [1], the plot is shown in Fig. 10. In this case, an R^2 value could not be obtained, as several values of K_s were 0, so the trendline could not be plotted. Based on these observations, it can be concluded that the new empirical model performs better in predicting stiffness than that in [1]. Although the R^2 of 0.3425 for the new empirical model is lower than the ideal threshold of 0.8, it still significantly outperforms the published prediction model for X-shaped screw arrangements.

Further comparisons were made by plotting the ratio of predicted/measured K_s *vs.* the angle (Fig. 11). It was found that the ratio for the published model ranges from 0 to 6.5. According to [1], the K_s values for specimens at 0° and 90° are always 0, but this did not hold, highlighting a key limitation of the published model. In contrast, the range of ratios for the new empirical model is between 0.5 and 4, which demonstrates a much better performance.

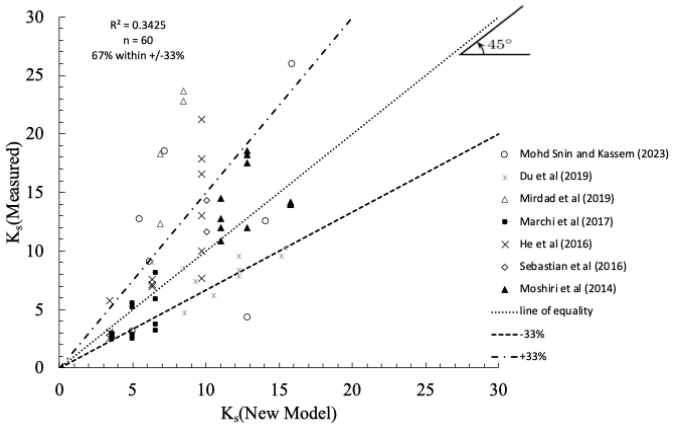

Figure 9. Measured *vs.* predicted K_s for the new empirical model
Source: Authors

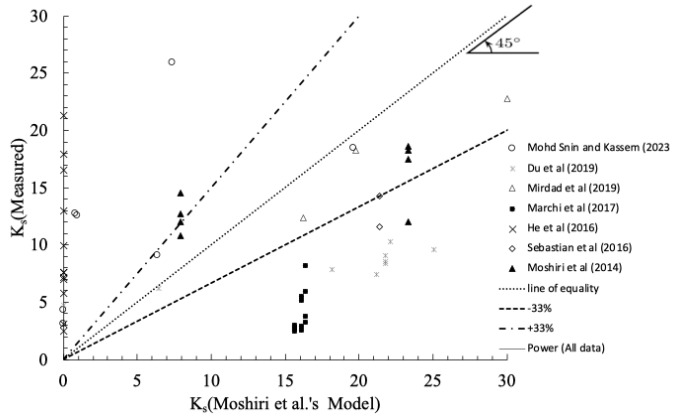

Figure 10. Measured *vs.* predicted K_s for the model in [1]
Source: Authors

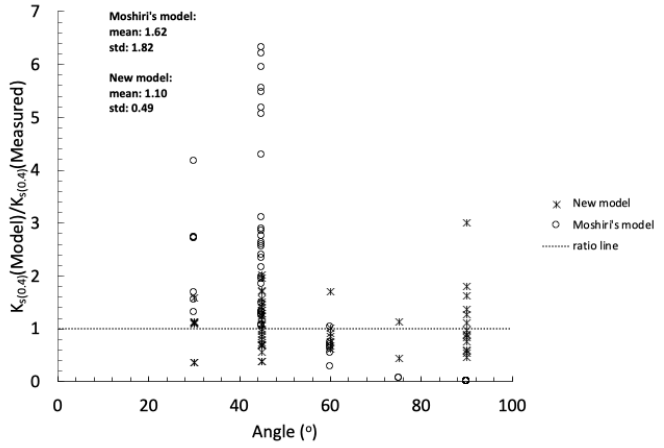

Figure 11. Model/measured K_s *vs.* screw angle
Source: Authors

Independent check using data from [1]

This section compares our shear force and stiffness models against those of [31] and [1] using 12 of their data samples. The mean and standard deviation of both models were calculated to facilitate comparison. Following these calculations, the ratio of model predictions to experimental values was plotted, as shown in Fig. 12 for the shear capacity. This parameter was better predicted by the new model, exhibiting a slightly better agreement with the measured values. The mean and standard deviation for the newly proposed model were 0.92 and 0.08, respectively, better than the values reported by [31], which had a mean of 1.06 and a standard deviation of 0.13. Fig. 13 presents the ratio of model predictions to experimental values for stiffness. It is clear that the new model offers a better prediction, with a mean and a standard deviation of 0.86 and 0.14, outperforming [1], which had a mean of 1.6 and a standard deviation of 0.91.

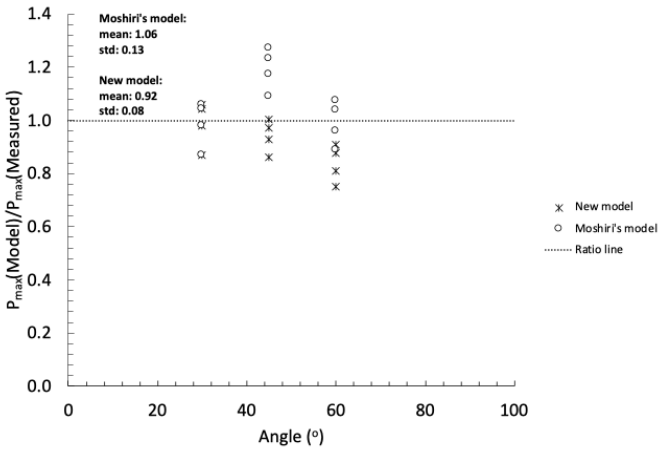

Figure 12. Model-predicted/measured P_{max} *vs.* screw angle using data from [31]
Source: Authors

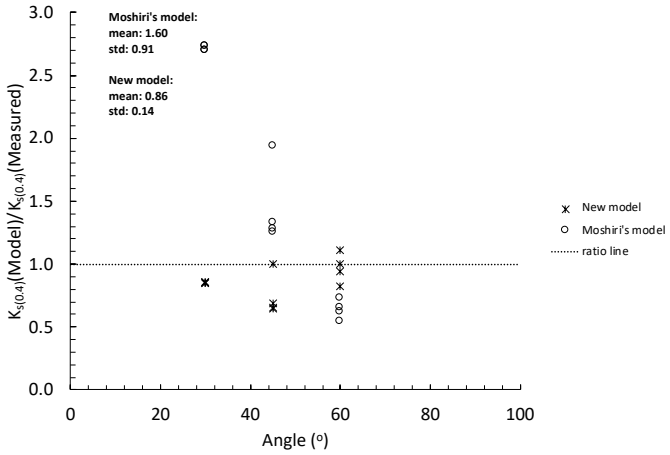

Figure 13. Model-predicted/measured K_s *vs.* screw angle using data from [1]
Source: Authors

Sensitivity analysis

This subsection discusses the influence of various parameters on the shear capacity and stiffness of screw connections in TCC structures. Five input variables, each with a range of values, were employed to conduct a comprehensive parametric analysis. The control variable method was applied, varying one parameter while the others remained constant. A sample from [1] served as the reference model (Table V). Furthermore, the ranges of the five input variables are provided in Table VI.

The analysis began by evaluating the effect of these parameters on the shear capacity. First, the impact of the length of the screw embedded in the concrete (L_c) on P_{max} was examined. The values of L_c considered were 65, 85, 95, and 100 mm. It was observed that the shear capacity of the connection increased significantly as L_c increased from 65 to 100 mm (Fig. 14). Next, we assessed the influence of timber beam strength (σ_B). The values considered were between 24, 30, 50, and 70 MPa. Fig. 15 presents a plot of P_{max} *vs.* σ_B, where a significant increase in shear capacity can be observed as σ_B increases.

Table V. Selected samples from the referenced model

Data sample	θ (°)	L_t (mm)	$\sigma_{y(s)}$ (MPa)	L_s (mm)	L_c (mm)	D (mm)	σ_S (MPa)	σ_B (MPa)	P_{max} (kN)
[1]	60	155	510	220	65	7.5	28	48	15

Source: Authors

Table VI. Parameter ranges

L_c (mm)	σ_S (MPa)	σ_B (MPa)	θ (°)	D (mm)
50-200	20-80	20-80	30-90	6-18

Source: Authors

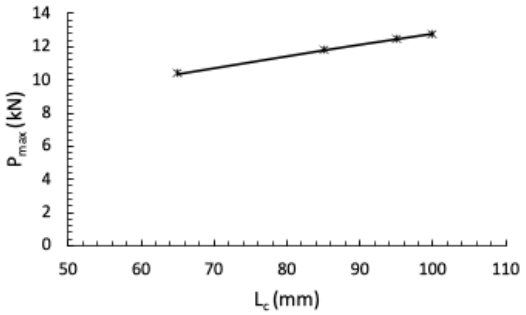

Figure 14. Influence of L_c on P_{max}
Source: Authors

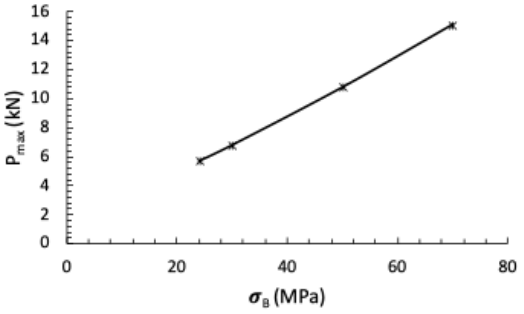

Figure 15. Influence of σ_B on P_{max}
Source: Authors

The analysis was further extended to consider the influence of concrete slab strength on shear capacity. Fig. 16 illustrates this effect, showing that the shear capacity of the connection increases with the concrete slab strength. Additionally, the sensitivity of P_{max} to the screw angle was examined, with Fig. 17 demonstrating that the screw angle has a relatively significant impact on the shear capacity. Lastly, Fig. 18 shows that the shear capacity increases significantly with larger screw diameters. For details related on Figs. 14-18, please refer to Appendix 2, which is provided as supplementary data.

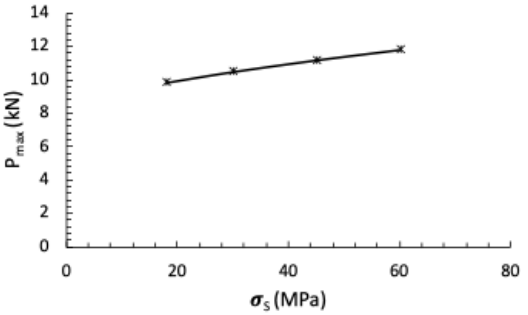

Figure 16. Influence of σ_S on P_{max}
Source: Authors

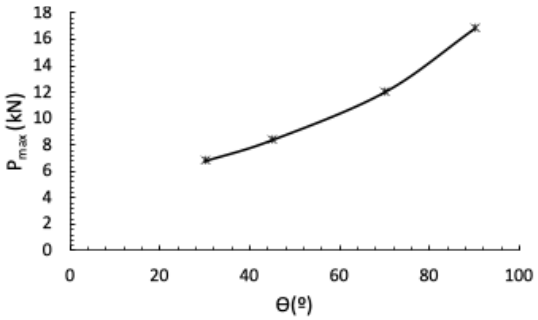

Figure 17. Influence of θ on P_{max}
Source: Authors

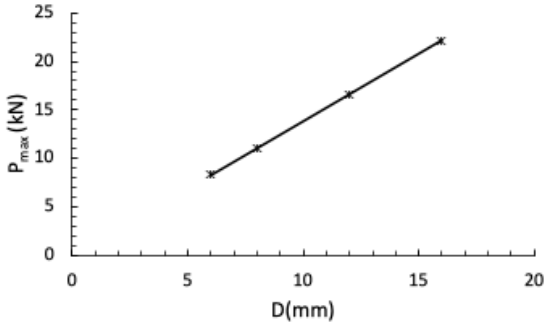

Figure 18. Influence of D on P_{max}
Source: Authors

Finally, the influence of the timber beam strength (σ_B), concrete slab strength (σ_S), and screw angle (θ) on the proposed stiffness model was evaluated using the same sample and ranges. As shown in Fig. 19, the stiffness of the connection increases significantly with the timber beam strength. Moreover, Fig. 20 indicates a decrease as the concrete slab strength increases, which may be due to microcracking at higher concrete strengths; when the screw experiences shear, higher-strength concrete can crack earlier due to brittleness, thereby reducing the effective stiffness [32]. Finally, the screw angle was found to have a notable influence on stiffness, which decreased as the former increased from 20° to 80° (Fig. 21). For additional details in this regard, please consult Appendix 2, which contains supplementary data.

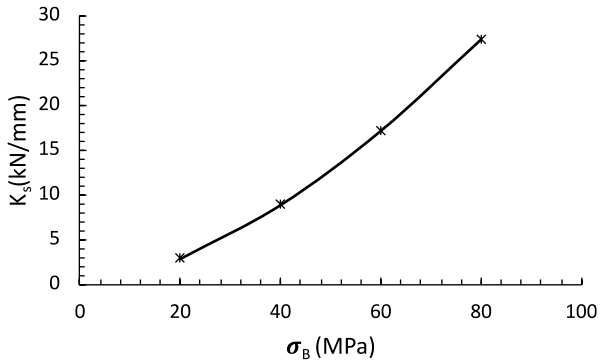

Figure 19. Influence of σ_B on K_S
Source: Authors

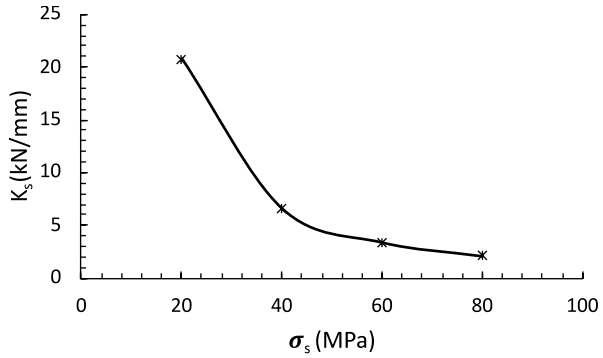

Figure 20. Influence of σ_S on K_s
Source: Authors

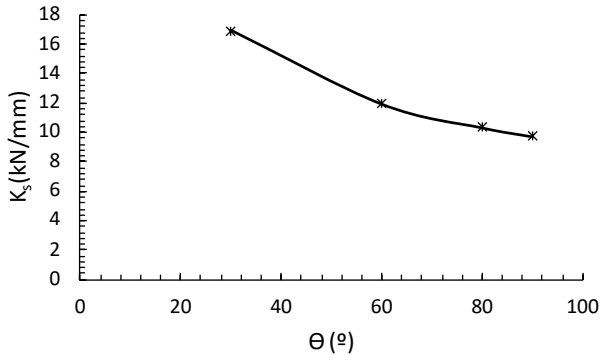

Figure 21. Influence of θ on K_s
Source: Authors

Conclusions

This paper presents empirical models for predicting the shear capacity and stiffness of TCC structures with X-shaped screw arrangements, which were developed via MLR analysis, utilizing a comprehensive database of 60 specimens. The model for shear capacity, shown in Eqs. (16) and (17), exhibits a strong predictive performance, with R^2 = 0.82 and 97% of specimens falling within ± 33% of the line of equality. Comparisons against a published model confirm the superior accuracy of our proposal. On the other hand, stiffness was calculated as 40% of the maximum load divided by the displacement, with the global flexibility coefficient identified as a key parameter. The resulting empirical stiffness model is given in Eq. (24). While the R^2 for predicted *vs.* measured K_s is 0.3425 (below the 0.8 threshold), our proposal outperforms the published model, whose R^2 could not be determined due to zero-stiffness predictions at 0° and 90°. The new model's stiffness ratio ranges from 0.5 to 4, whereas the other model reports a range of 0-6.5, indicating the superior predictive performance of the latter.

Acknowledgements

The authors acknowledge the funding received from Universiti Sains Malaysia under the short-term grant 304/PAWAM/6315691, which helped to support this research.

Conflicts of interest

The authors confirm that this work is original and has not been published elsewhere, nor is it currently under consideration for publication elsewhere. The authors declare that they have no conflict of interest.

Data availability

The datasets generated and/or analyzed during the current study are available from the corresponding author upon reasonable request.

CRediT author statement

MAMS was in charge of conceptualization, supervision, and validation. This author provided critical feedback and wrote the main part of the manuscript. AHG was in charge of data collection, developed the workflow, and performed assessments. DHL was in charge of data collection and led the drafting process.

References

[1] F. Moshiri, R. Shrestha, and K. Crews, "The predictive model for stiffness of inclined screws as shear connection in timber-concrete composite floor," in *Materials and Joints in Timber Structures*, S. Aicher, H. W. Reinhardt, and H. Garrecht, Eds. Dordrecht, Netherlands: Springer, 2014, pp. 443–453. https://doi.org/10.1007/978-94-007-7811-5_40

[2] A. Ogrin and T. Hozjan, "Timber-concrete composite structural elements," *Engineered Wood Products for Construction*, M. Gong, Ed. London, UK: IntechOpen, 2022. https://doi.org/10.5772/intechopen.99624

[3] A. Pogoreltsev, S. Turkovsky, and V. Stoyanov, "Rigid joints on glued-in rods of bending and compression-bending elements of large-span laminated timber structures," in *World Conf. Timber Eng. (WCTE 2023)*, 2023, pp. 4201–4208. https://doi.org/10.52202/069179-0546

[4] J. Estévez-Cimadevila, E. Martín-Gutiérrez, F. Suárez-Riestra, D. Otero-Chans, and J. A. Vázquez-Rodríguez, "Timber-concrete composite structural flooring system," *J. Build. Eng.*, vol. 49, art. 104078, 2022. https://doi.org/10.1016/j.jobe.2022.104078

[5] A. Romero, J. Yang, F. Hanus, H. Degée, and C. Odenbreit, "Push-out tests on connections for demountable and reusable steel-timber composite beam and flooring systems," *World Conf. Timber Eng. (WCTE 2023)*, 2023, pp. 3568–3574. https://doi.org/10.52202/069179-0464

[6] V. Bajzecerova, M. Kovac, and J. Kanocz, "Structural analysis of cross-laminated timber slabs subjected to bending – State of the art," *Select. Sci. Papers J. Civil Eng.*, vol. 13, no. 1, pp. 133–140, 2018. https://doi.org/10.1515/sspjce-2018-0027

[7] H. Du, X. Hu, Z. Sun, and W. Fu, "Shear stiffness of inclined screws in timber–concrete composite beam with timber board interlayer," *Adv. Struct. Eng.*, vol. 23, no. 16, pp. 3555–3565, 2020. https://doi.org/10.1177/1369433220940814

[8] V. S. Pham, "Shear behavior of different connections for cross-laminated timber-concrete composite floor," 2022. [Online]. Available: https://doi.org/10.2139/ssrn.4229164

[9] M. W. Hammad, H. R. Valipour, and S. J. Foster, "Timber-concrete composites (TCC) floors subjected to hogging moment," *Eng. Struct.*, vol. 303, art. 117488, 2024. https://doi.org/10.1016/j.engstruct.2024.117488

[10] J. Pyykkö and S. Svensson, "Load-bearing capacity of slender dowel-type fasteners in Timber-Concrete Composite connections," *Eng. Struct.*, vol. 316, art. 118556, 2024. https://doi.org/10.1016/j.engstruct.2024.118556

[11] R. Hassan, A. Ibrahim, and Z. Ahmad, "Load-carrying capacity of timber joints," in *Timber Connections*. Singapore: Springer, 2023, pp. 43–52. https://doi.org/10.1007/978-981-19-2697-6_4

[12] Z. Tekic, and S. Djordjevic, "Experimental determination of load bearing capacity of connections realized by punched metal plate fastener," *Tehnika*, vol. 69, no. 5, pp. 735–741, 2014. https://doi.org/10.5937/tehnika1405735t

[13] R. Tomasi, A. Crosatti, M. Piazza, "Theoretical and experimental analysis of timber-to-timber joints connected with inclined screws," *Const. Build. Mater.*, vol. 24, no. 9, pp. 1560–1571, 2010. https://doi.org/10.1016/j.conbuildmat.2010.03.007

[14] S. Esmaeildoust, D. Tomlinson, and Y. H. Chui. "Performance of Timber-Concrete Composite (TCC) Systems Connected with Inclined Screws: A Literature Review," *J. Comp. Sci.*, vol 9, no. 1, art. 13, 2025. https://doi.org/10.3390/jcs9010013

[15] I. B. Johari, M. A. B. Mohd Snin, S. F. B. Senin, and M. R. B. Mohamad Rashid, "Screw connection systems in timber-concrete composite structures: A literature review," *Tehnički Vjesnik*, vol. 30, no. 4, pp. 1336–1346, 2023. https://doi.org/10.17559/TV-20220820075553

[16] I. Bejtka, and H. J. Blaß, "Joints with inclined screws," presented at *Meet. 35 Int. Coun. Build Res. Stud. Doc.*, Kyoto, Japan, 2002.

[17] X. Sun, Z. Gan, Z. Li and M. He, "Shear performance of inclined crossing screws for nail-laminated timber-concrete composite floor with an OSB interlayer," *Const. Build. Mater.*, vol. 458, art. 139621, 2025. https://doi.org/10.1016/j.conbuildmat.2024.139621

[18] M. Zeman, P. Sejkot, K. Mikes, M. Fragiacomo, and A. Aloisio, "Glued-in steel plate and screwed connections in timber–concrete composites systems: Mechanical performance and design implications," *J. Build. Eng.*, vol. 96, art. 110477, 2024. https://doi.org/10.1016/j.jobe.2024.110477

[19] CEN, *Eurocode 5: Design of timber structures – Part 1-1: General – Common rules and rules for buildings* (EN 1995-1-1:2021). Brussels, Belgium: European Committee for Standardization, 2021.

[20] G. He, H. Xiao, L. Chen, and L. Li, "The performance study of notch-stud connections of timber-concrete composite beam: The performance study of notch-stud connections of timber-concrete composite beam," in *Adv. Energy Environ. Mater. Sci. Proc. 2nd Int. Conf. Energy Environ. Materi. Sci. (EEMS 2016)*, 2016, pp. 475–479.

[21] M. Molina Herrera and X. F. Hurtado Amézquita, "Formulating a design for a screw-type shear connector in a composite section," *Ing. Investig.*, vol. 31, no. 2, pp. 52–64, 2011. https://doi.org/10.15446/ing.investig.v31n2.23465

[22] J. Skinner, J. Bregulla, R. Harris, K. Paine, and P. Walker, "Screw connectors for thin topping, timber–concrete composites," *Mater. Struct.*, vol. 47, no. 11, pp. 1891–1899, 2013. https://doi.org/10.1617/s11527-013-0158-6

[23] W. M. Sebastian, J. Mudie, G. Cox, M. Piazza, R. Tomasi, and I. Giongo, "Insight into mechanics of externally indeterminate hardwood–concrete composite beams," *Const. Build. Mater.*, vol. 102, pp. 1029–1048, 2016. https://doi.org/10.1016/j.conbuildmat.2015.10.015

[24] M. A. Mohd Snin, and M. M. Kassem, "Novel use of scanning methods to investigate the performance of screw connections in timber-concrete composite structures," *Adv. Civil Eng.*, vol. 2023, art. 4176805, 2023. https://doi.org/10.1155/2023/4176805

[25] A. M. Harte, "Introduction to timber as an engineering material," in *ICE Manual of Construction Materials*, M. Forde, Ed. Leeds, UK: Emerald Publishing Limited, 2009, vol. 2, pp. 707–716. https://doi.org/10.1680/mocm.35973

[26] CEN, *Eurocode 2: design of concrete structures. Part 2, Concrete bridges: design and detailing rules*. Singapore: Springer Singapore, 2012.

[27] P. Gelfi, E. Giuriani, and A. Marini, "Stud shear connection design for composite concrete slab and wood beams," *J. Struct. Eng.*, vol. 128, no. 12, pp. 1544–1550, 2002. https://doi.org/10.1061/(asce)0733-9445(2002)128:12(1544)

[28] L. Marchi, R. Scotta, and L. Pozza, "Experimental and theoretical evaluation of TCC connections with inclined self-tapping screws," *Mater. Struct.*, vol. 50, no. 3, art 180, 2017. https://doi.org/10.1617/s11527-017-1047-1

[29] H. Du, X. Hu, Z. Xie, and H. Wang, "Study on shear behavior of inclined cross lag screws for glulam-concrete composite beams," *Const. Build. Mater.*, vol. 224, pp. 132–143, 2019. https://doi.org/10.1016/j.conbuildmat.2019.07.035

[30] M. A. Mirdad and Y. H. Chui, "Load-slip performance of Mass Timber Panel-Concrete (MTPC) composite connection with Self-tapping screws and insulation layer," *Const. Build. Mater.*, vol. **213**, pp. 696–708, 2019. https://doi.org/10.1016/j.conbuildmat.2019.04.117

[31] F. Moshiri, C. Gerber, H. Valipour, R. Shrestha, and K. Crews, "The predictive model for strength of inclined screws as shear connection in timber-concrete composite floor," in *Proc. 22nd Australasian Conf. Mech. Struct. Mater. (ACMSM 2012)*, 2013, pp. 1059–1064. https://espace.library.uq.edu.au/view/UQ:0560957

[32] A. Ceccotti, "Composite concrete-timber structures," *Prog. Struct. Eng. Mater.*, vol. 4, no. 3, pp. 264–275, 2002. https://doi.org/10.1002/pse.126

Appendix 1

Source	Θ	L_t (mm)	$\sigma_{y(s)}$ (MPa)	L_s (mm)	L_c (mm)	l_c (mm)	D (mm0)	σ_S (MPa)	ρ_s (kg/m³)	ρ_t (kg/m³)	σ_B MPa	$K_{s(40)}$ (kN/mm) per fastener	P_{max} (kN) per fastener
Mohd Snin and Kassem (2023)	30	130	820	210	80	28.62	6	26.5	2400	740	70	21.0	20.5
	60	160	820	210	50	12.19	6	26.5	2400	740	70	25.9	16.8
	75	152	820	210	58	10.83	6	26.5	2400	740	70	12.5	14.3
	90	147	820	210	63	9.85	6	26.5	2400	740	70	4.3	22.3
	45	125	820	210	85	25.57	6	16.36	2400	420	24	18.5	9.9
	60	125	820	210	85	20.72	6	16.36	2400	420	24	9.1	8.0
	75	125	820	210	85	15.88	6	16.36	2400	420	24	12.7	8.2
	90	125	820	210	85	13.29	6	16.36	2400	420	24	3.1	10.9
Sebastian et al (2016)	45	150	1000	210	60	18.05	6	32.7	2400	740	59.4	11.6	19.5
	45	150	1000	210	60	18.05	6	32.7	2400	740	59.4	14.3	16.0
He et al (2016)	90	80	1200	120	40	6.25	8	49.7	2400	552.1	44.9	5.7	15.4
	90	80	1200	120	40	6.25	8	49.7	2400	552.1	44.9	3.1	13.8
	90	80	1200	120	40	6.25	8	49.7	2400	552.1	44.9	2.5	12.0
	90	80	1200	120	40	6.25	12	49.7	2400	552.1	44.9	7.6	19.7
	90	80	1200	120	40	6.25	12	49.7	2400	552.1	44.9	7.1	25.2
	90	80	1200	120	40	6.25	12	49.7	2400	552.1	44.9	7.0	14.5
	90	80	1200	120	40	6.25	16	49.7	2400	552.1	44.9	21.3	29.4
	90	80	1200	120	40	6.25	16	49.7	2400	552.1	44.9	17.9	32.8
	90	80	1200	120	40	6.25	16	49.7	2400	552.1	44.9	7.6	29.8
	90	60	1200	100	40	6.25	16	49.7	2400	552.1	44.9	16.5	27.3
	90	60	1200	100	40	6.25	16	49.7	2400	552.1	44.9	13.0	24.3
	90	60	1200	100	40	6.25	16	49.7	2400	552.1	44.9	10.0	27.9
Marchi et al (2017)	45	80	400	160	80	24.06	8	32.73	2400	426	24	3.0	8.5
	45	80	400	160	80	24.06	8	32.73	2400	426	24	2.9	7.8
	45	80	400	160	80	24.06	8	32.73	2400	426	24	2.6	8.2
	45	80	400	160	80	24.06	8	32.73	2400	426	24	2.5	7.8
	45	80	400	160	80	24.06	10	32.73	2400	426	24	5.2	9.9
	45	80	400	160	80	24.06	10	32.73	2400	426	24	2.9	11.0
	45	80	400	160	80	24.06	10	32.73	2400	426	24	5.6	10.6
	45	80	400	160	80	24.06	10	32.73	2400	426	24	2.5	10.5
	45	80	400	160	80	24.06	12	32.73	2400	426	24	8.2	13.1
	45	80	400	160	80	24.06	12	32.73	2400	426	24	5.9	12.8
	45	80	400	160	80	24.06	12	32.73	2400	426	24	3.8	13.6
	45	80	400	160	80	24.06	12	32.73	2400	426	24	3.2	13.3
Du et al (2019)	45	110	462	180	70	21.06	12	40	2400	491	43.4	8.4	19.8
	45	110	462	180	70	21.06	12	50	2400	491	43.4	8.6	21.8
	45	110	462	180	70	21.06	12	60	2400	491	43.4	9.1	24.6
	45	110	462	180	70	21.06	10	40	2400	491	43.4	7.4	17.7
	45	110	462	180	70	21.06	14	40	2400	491	43.4	10.3	22.2
	45	90	462	180	90	27.07	12	40	2400	491	43.4	7.8	18.0
	45	130	462	180	50	15.04	12	40	2400	491	43.4	9.6	23.4
	30	110	462	180	70	25.05	12	40	2400	491	43.4	9.6	23.5
	60	110	462	180	70	17.07	12	40	2400	491	43.4	6.2	17.8
	90	110	462	180	70	10.94	12	40	2400	491	43.4	4.8	19.4
Mirdad et al. (2019)	45	80	1000	150	70	21.06	11	39	2400	504	32	12.4	16.8
	30	80	1000	150	70	25.05	11	39	2400	504	32	22.8	20.9
	45	100	1000	200	100	30.08	11	39	2400	504	32	18.3	22.2
	30	100	1000	200	100	35.78	11	39	2400	504	32	23.7	19.8
Moshiri et al (2014)	60	155	510	220	65	15.85	7.5	28	2400	560	48	12.8	17.5
	60	155	510	220	65	15.85	7.5	28	2400	560	48	10.8	16.3
	60	155	510	220	65	15.85	7.5	28	2400	560	48	12.0	15.0
	60	155	510	220	65	15.85	7.5	28	2400	560	48	14.5	14.5
	45	142	510	220	78	23.46	7.5	28	2400	560	48	17.5	17.5
	45	142	510	220	78	23.46	7.5	28	2400	560	48	18.6	16.3
	45	142	510	220	78	23.46	7.5	28	2400	560	48	18.2	15.5
	45	142	510	220	78	23.46	7.5	28	2400	560	48	12.0	15.0
	30	123	510	220	97	34.71	7.5	28	2400	560	48	14.2	22.5
	30	123	510	220	97	34.71	7.5	28	2400	560	48	14.2	20.0
	30	123	510	220	97	34.71	7.5	28	2400	560	48	14.0	18.5
	30	123	510	220	97	34.71	7.5	28	2400	560	48	14.0	18.8

Appendix 2

Table A2a. Details of data for Figure 14

Angle (θ)	D (mm)	L_c (mm)	L_t (mm)	l_c (mm) (5)	σ_B (MPa)	σ_S (MPa)	$f_{h,c}$ (MPa) (14)	$P_{a(c)}$ (kN) (3)	$P_{a(t)}$ (kN) (2)	P_b (kN) (15)	P_{max} (kN) (16) or (17)
60	7.5	65	155	16.9	48	28	26.34	2.14	8.14	8.23	10.37
60	7.5	85	155	22.1	48	28	21.95	2.80	8.14	8.96	11.77
60	7.5	95	155	24.7	48	28	20.35	3.13	8.14	9.29	12.42
60	7.5	100	155	26	48	28	19.65	3.30	8.14	9.44	12.74

*In bracket ( ) : Equation used for calculation

Table A2b. Details of data for Figure 15

Angle (θ)	D (mm)	L_c (mm)	L_t (mm)	l_c (mm) (5)	σ_B (MPa)	σ_S (MPa)	$f_{h,c}$ (MPa) (14)	$P_{a(c)}$ (kN) (3)	$P_{a(t)}$ (kN) (2)	P_b (kN) (15)	P_{max} (kN) (16) or (17)
60	7.5	65	155	16.9	24	28	11.46	2.14	4.67	3.58	5.72
60	7.5	65	155	16.9	30	28	14.98	2.14	5.59	4.68	6.82
60	7.5	65	155	16.9	50	28	27.66	2.14	8.41	8.64	10.78
60	7.5	65	155	16.9	70	28	41.42	2.14	11.00	12.94	15.08

*In bracket ( ) : Equation used for calculation

Table A2c. Details of data for Figure 16

Angle (θ)	D (mm)	L_c (mm)	L_t (mm)	l_c (mm) (5)	σ_B (MPa)	σ_S (MPa)	$f_{h,c}$ (MPa) (14)	$P_{a(c)}$ (kN) (3)	$P_{a(t)}$ (kN) (2)	P_b (kN) (15)	P_{max} (kN) (16) or (17)
60	7.5	65	155	16.9	48	18	26.34	1.59	8.14	8.23	9.82
60	7.5	65	155	16.9	48	30	26.34	2.24	8.14	8.23	10.47
60	7.5	65	155	16.9	48	45	26.34	2.94	8.14	8.23	11.17
60	7.5	65	155	16.9	48	60	26.34	3.57	8.14	8.23	11.80

*In bracket ( ) : Equation used for calculation

Table A2d. Details of data for Figure 17

Angle (θ)	D (mm)	L_c (mm)	L_t (mm)	l_c (mm) (5)	σ_B (MPa)	σ_S (MPa)	$f_{h,c}$ (MPa) (14)	$P_{a(c)}$ (kN) (3)	$P_{a(t)}$ (kN) (2)	P_b (kN) (15)	P_{max} (kN) (16) or (17)
30	7.5	65	155	24.7	48	28	20.35	3.71	14.08	3.07	6.78
45	7.5	65	155	20.8	48	28	22.87	3.03	11.50	5.36	8.39
70	7.5	65	155	14.3	48	28	29.51	1.47	5.57	10.54	12.01
90	7.5	65	155	9.1	48	28	40.12	0.00	0.01	16.82	16.82

*In bracket ( ) : Equation used for calculation

Table A2e. Details of data for Figure 18

Angle (θ)	D (mm)	L_c (mm)	L_t (mm)	l_c (mm) (5)	σ_B (MPa)	σ_S (MPa)	$f_{h,c}$ (MPa) (14)	$P_{a(c)}$ (kN) (3)	$P_{a(t)}$ (kN) (2)	P_b (kN) (15)	P_{max} (kN) (16) or (17)
60	6	65	155	16.9	48	28	26.34	1.71	6.51	6.58	8.29
60	8	65	155	16.9	48	28	26.34	2.29	8.68	8.77	11.06
60	12	65	155	16.9	48	28	26.34	3.43	13.02	13.16	16.59
60	16	65	155	16.9	48	28	26.34	4.57	17.36	17.55	22.12

*In bracket ( ) : Equation used for calculation

Table A2e. Details of data for Figure 19

Angle (θ)	D (mm)	Lc (mm)	Lt (mm)	σ_B (mm)	σ_S (mm)	E_s (MPa)	I_s (mm⁴)	K_s (kN/mm) (24)
60	7.5	65	155	20	28	205000	155.24	2.89
60	7.5	65	155	40	28	205000	155.24	8.89
60	7.5	65	155	60	28	205000	155.24	17.15
60	7.5	65	155	80	28	205000	155.24	27.33

*In bracket ( ) : Equation used for calculation

Table A2f. Details of data for Figure 20

Angle (θ)	D (mm)	Lc (mm)	Lt (mm)	σ_B (mm)	σ_S (mm)	E_s (MPa)	I_s (mm⁴)	K_s (kN/mm) (24)
60	7.5	65	155	48	20	205000	155.24	20.75
60	7.5	65	155	48	40	205000	155.24	6.66
60	7.5	65	155	48	60	205000	155.24	3.42
60	7.5	65	155	48	80	205000	155.24	2.14

*In bracket ( ) : Equation used for calculation

Table A2f. Details of data for Figure 21

Angle (θ)	*D* (mm)	*Lc* (mm)	*Lt* (mm)	σ_B (mm)	σ_S (mm)	E_s (MPa)	I_s (mm⁴)	K_s (kN/mm) (24)
30	7.5	65	155	48	28	205000	155.24	16.90
60	7.5	65	155	48	28	205000	155.24	11.95
80	7.5	65	155	48	28	205000	155.24	10.35
90	7.5	65	155	48	28	205000	155.24	9.76

*In bracket ( ) : Equation used for calculation